Journal of Power Sources 196 (2011) 1019–1029

Contents lists available at ScienceDirect

Journal of Power Sources

journal homepage: www.elsevier.com/locate/jpowsour

Study on local morphological changes of nickel in solid oxide fuel cell anode using porous Ni pellet electrode

Zhenjun Jiao [a,*], Norikazu Takagi [a], Naoki Shikazono [a], Nobuhide Kasagi [b]

[a] Institute of Industrial Science, University of Tokyo, 4-6-1 Komaba, Meguro-ku, Tokyo 153-8505, Japan
[b] Department of Mechanical Engineering, University of Tokyo, Bunkyo-ku, Tokyo 113-8656, Japan

ARTICLE INFO

Article history:
Received 4 March 2010
Received in revised form 17 August 2010
Accepted 18 August 2010
Available online 26 August 2010

Keywords:
SOFC
TPB deposition
Ni redistribution
Ni droplet
Interlock

ABSTRACT

Morphological change of nickel, especially the aggregation of nickel, in solid oxide fuel cell anode is an important deactivation mechanism which results in long-period degradation of anode. In order to study the mechanisms which cause local morphological changes of nickel in solid oxide fuel cell anode, porous nickel pellet, which is mechanically pressed against dense YSZ pellet with LSM cathode, was employed as the anode of the cell. The cell was tested by static-potential method in hydrogen with different humidities environment for 60 h. The study focused on the vicinity of three phase boundary which concentrated at nickel–YSZ interface. After the discharging test, the cell performance and the microstructure at nickel–YSZ contacting point of interface were studied and correlated to nickel morphological changes. The interlocking effect and the spreading of densified nickel layer phenomena were observed between nickel and YSZ substrate after discharging with an anode to cathode terminal voltage of 0.6 V. Humidity enhanced nickel surface diffusion and humidity gradient driving vaporization–deposition mechanism, which caused the growing and merging of independent nickel droplets, were used to explain the local morphological changes and redistribution of nickel inside and along the edge of YSZ surface bonded nickel cluster, respectively. The bulk nickel morphological changes were also studied to support the humidity enhanced nickel surface diffusion mechanism. The competition of interlocking effect, nickel redistribution at TPB and bulk nickel sintering finally determined the cell performance.

1. Introduction

Solid oxide fuel cell (SOFC) has been emerged as an attractive device because of its advantages such as fuel flexibility and high efficiency. The current challenge focuses on the long-time stability and durability of SOFC electrodes. In the stationary applications, more than 40,000 h lifetime is generally required. The SOFC anode exhibits slow degradation in long-time discharging experiments with nickel (Ni, hereafter) coarsening, which can be explained by particle sintering [1]. With higher current density or overpotential, rapid degradation or even sudden failing of the cell is observed [2]. Generally speaking, the performance degradation and failure are correlated to the electrode reaction mechanisms. In conventional SOFC anodes, porous Ni–YSZ cermet is widely used, while Ni exhibits certain morphological changes at the cell operating temperature. Thus, great efforts have been payed to investigate the factors which influence the anode aging process.

Simwonis et al. [3] studied the coarsening of Ni particles in porous anode and correlated the changes in electrical conductivity with the microstructural parameters. A large decrease in electrode electrical conductivity was observed in 4000 h exposure in humidified hydrogen without discharging, which can be explained by the increase of average Ni particle size from 2 to 2.6 μm. Koch et al. [1] tested the performance and degradation of SOFC under several operating conditions. A critical anode–cathode voltage was found to be around 0.75 V, below which the degradation rates were significant. The same result has also been proved by Matsui et al. [2], and at the same time, the influence of fuel humidity was observed to be significant on the performance and stability of Ni–YSZ cermet anode. In their experiments, sudden failure of the cell was observed when the fuel humidity was 40%. Rapid microstructure change of Ni was observed. It can be concluded that some factors other than sintering of Ni may cause degradation or even sudden death of the SOFC anode. The possible reasons can be attributed to the local degradation at three phase boundary (TPB, hereafter). However, the elementary nature of the reaction steps at TPB is still unclear. Goodwin et al. [4] predicted that the effective distance from TPB is below 100 nm, and out of this distance the reaction rates are independent of position because of the equilibrium established between solid surface and gas phase. Marcel et al. [5] built their model for surface

* Corresponding author. Tel.: +81 354526777; fax: +81 354526777.
E-mail addresses: zhenjun@iis.u-tokyo.ac.jp (Z. Jiao), shika@iis.u-tokyo.ac.jp (N. Shikazono).

0378-7753/$ – see front matter © 2010 Elsevier B.V. All rights reserved.
doi:10.1016/j.jpowsour.2010.08.047

transport process and concluded that the reactants concentrations near TPB may largely deviate from those derived from thermodynamical equilibrium considerations. This supports the assumption of local degradation at TPB. Hansen et al. [6] studied the Ni–YSZ interaction along TPB by using Ni wire as a simplified anode. A film of impurities was found at Ni–YSZ interface while impurity ridges were also found at TPB. At the same time, Ni redistribution was found to form hill and valley structures in sub-micron scale at the contacting area. Several kinds of impurities were found in the ridge along TPB, which made the local reaction even more complex. In their study, no model was proposed to explain the local morphological change of Ni. In order to elucidate the reaction mechanism with pure Ni, Mazusaki et al. [7] employed Ni stripe pattern electrodes prepared on the surface of YSZ with well defined morphology. The rate of anodic reaction was found to be determined by the reaction of hydrogen and the absorbed oxygen on Ni surface. From the literature, it can be concluded that the long-period degradation of Ni–YSZ cermet anode is due to Ni migration [1,8,9] which can cause the coarsening of Ni network. According to the authors' knowledge, no systematical work has been carried out to study the local morphological changes of Ni and correlate them to cell performances.

In this paper, a porous Ni pellet which was mechnically pressed against the dense YSZ electrolyte pellet, with LSM cathode screen-printed, was employed as an anode. The study focuses on the local morphological changes of Ni at Ni–YSZ interface. Compared to normal Ni–YSZ composite anode, this new method has the advantage of easy observation of the reaction sites at Ni–YSZ interface, which facilitates the correlation of phase changes to cell performances. In addition, this method can also be applied to observe the influences of operating gas environment on bulk Ni particle simultaneously [6,7,10].

2. Experimental devices

2.1. Preparation of experimental materials

NiO powder used in this study has an average particle diameter of 1.1 μm. The powder was then ball milled with 10 wt% organic pore former in ethanol for 24 h and dried in air at 200 °C. The porous NiO pellets were obtained by uniaxial-pressing in a steel die of a diameter 20 mm at a pressure of 20 MPa. The pressed pellets were then sintered at 1400 °C for 3 h to get porous NiO pellets with a diameters of 16 mm and a thickness of 0.5 mm.

$(La_{0.8}Sr_{0.2})_{0.97}MnO_3$ (LSM) powder (0.4 μm) was used as cathode material. The powder was mixed with the terpineol solvent and the ethylcellulose binder in agate mortar to obtain cathode printing slurry. And the slurry was screen-printed onto commercial dense YSZ pellet (diameter 20 mm, thickness 0.5 mm) with a diameter of 10 mm. After screen printing, the cathode was sintered at 1150 °C for 3 h.

2.2. Fuel cell measurement system

The SOFC performance measurement setup is shown in Fig. 1. Pt meshes was used as current collectors, which were pressed against the electrodes by springs connected to alumina tubes. Glass rings were used as seals between two outer alumina tubes, and the two outer tubes were also pressed against the cell by springs. The YSZ pellet was surrounded by a Pt wire as reference electrode. Pt paste was used to enhance the conductive connection between Pt wire and YSZ pellet. Nitrogen was used as the protective gas in the initial heating up stage. After the furnace temperature had been increased to 600 °C, glass seals started to melt and covered both edges of the cell, the reference electrode and two outer tube edges,

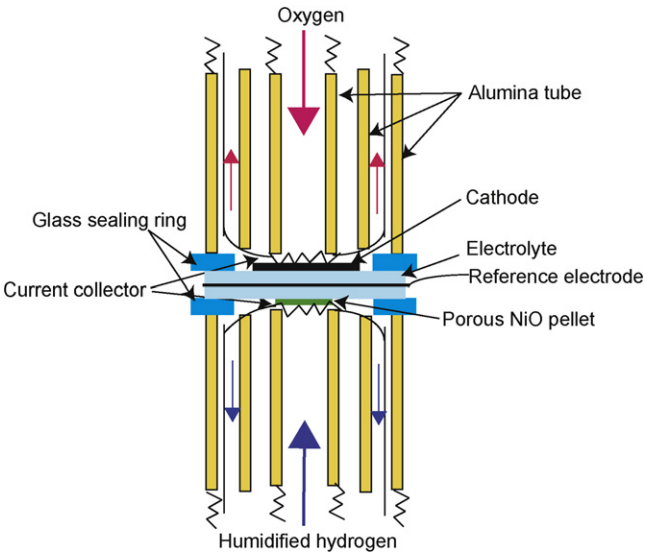

Fig. 1. Schematic of SOFC measurement setup.

which resulted in good sealing. Then, dry hydrogen gas (50 sccm) was introduced to reduce the porous NiO pellet for 1 h before cell testing was conducted. The performance of SOFC was evaluated at 800 °C by using humidified hydrogen as a fuel and pure oxygen as an oxidant (50 sccm for both anode and cathode). H_2O bubbler was used to control the fuel humidity. In order to enhance the local electrochemical reactions at TPB, low terminal voltages were applied in the cell potential-static discharging experiments [1].

Cell impedance spectra (frequency range 1–10^5 Hz) measurements were conducted with a Solatron frequency analyzer (1255B) and a Solatron interface via current collectors. As shown in Fig. 2, anode–cathode (A–C) and cathode–reference (C–R) impedance was measured within standard gas environment (anode: 3% H_2O, 97% H_2; cathode: pure O_2). By comparing the A–C and C–R impedance spectra, it is seen that the cell performance is dominated by anode and cathode contributed to less than 3% of the total cell ohmic resistance and activation polarization. With a standard sintering process, cathode with stable performance can be obtained and in order to minimize the errors caused by the position of reference wire and the Pt soldering paste on such a thin YSZ pellet, A–C static terminal potential method was applied to measure the cell performances.

2.3. Image processing

Observation of the microstructure is facilitated by FIB-SEM (Carl Zeiss, NVision40). The elements analysis was accomplished

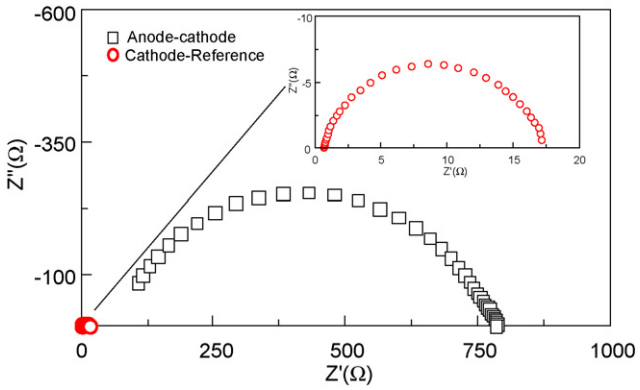

Fig. 2. Anode–cathode and reference–cathode impedance before discharging.

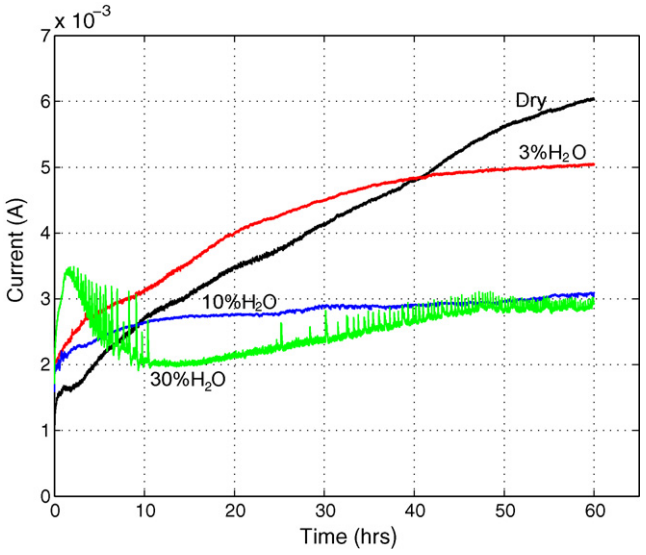

Fig. 3. Cell performances measured in different humidified hydrogen with potential-static method (A–C terminal voltage, 0.6 V).

by energy dispersive X-ray spectroscopy (EDX; Thermo Electron, NSS300). Cross-section of sample to be observed was polished by Ar-ion beam cross-section polisher (JEOL Ltd., SM-09010), which provides less damage and smoother cross-section compared to the diamond slurry polishing.

3. Experimental results

3.1. Cell performances within different humidified environments

Four humidity conditions, dry, 3% H_2O, 10% H_2O and 30% H_2O, were applied at anode side in discharging processes. Fig. 3 shows the transient performances of the four cells with a discharging time of 60 h. Because of the uncertain contacting area between Ni and YSZ, absolute current values were used instead of current densities to describe the transient cell performances tendencies. The initial current of the cell tested in dry hydrogen was lower than the other three cells, which presented similar initial currents. This is caused by the higher activation polarization without the presence of humidity in hydrogen [11]. It can be seen that the performances of the cell within dry, 3% H_2O and 10% H_2O conditions kept increasing in 60 h. The increasing rates in dry hydrogen and 3% H_2O are much faster than in 10% H_2O. After 60 h discharging, output current value in dry hydrogen increased to 4 times and 3% H_2O increased to 2.5 times of the initial value, while that in 10% H_2O increased by about 50%. In 30% H_2O, rapid increase of performance was observed at the beginning of discharging. But after about 2 h, its performance started to become very irregular. Every discharging experiments were repeated several times to confirm the reproducibility of the experimental results.

3.2. Morphological change of Ni

After the measurements, the system was cooled down to room temperature with continuous hydrogen flow supplied to anode side. The porous Ni pellet was found to attach to YSZ substrate with strong mechanical strength for all the four testing cases. By peeling off the Ni pellet from YSZ substrate, it was found that Ni pellets were all bonded to the YSZ surface as clusters at several contacting points. The typic microstructures of both bonded Ni cluster and broken porous Ni pellet of the sample tested in hydrogen with 3% H_2O were observed by SEM with different magnifications, as shown in Fig. 4. In Fig. 4(a), large amount of smooth densified Ni layer was observed along the edge of bonded Ni cluster. Most of the Ni layer were connected to the main Ni cluster while a few droplets were observed as independent islands. Fig. 4(b) shows the corresponding microstructures of the Ni pellet which was broken.

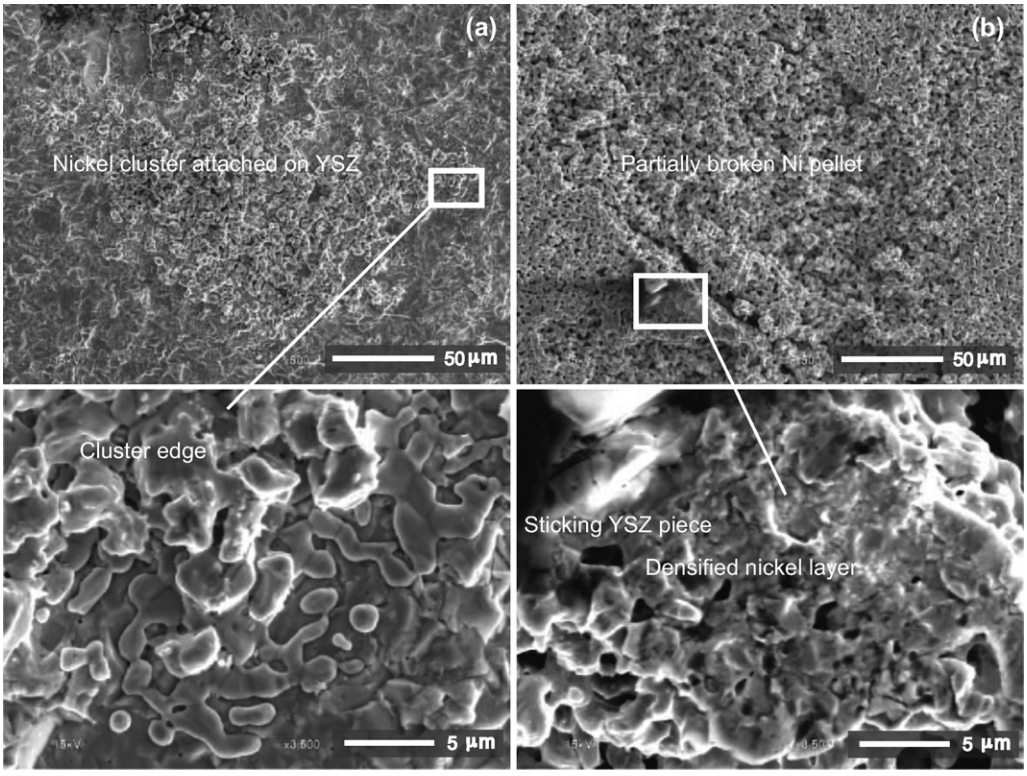

Fig. 4. (a) YSZ surface with Ni clusters bonded and satellite Ni droplets after 60 h discharging in 3% H_2O hydrogen and (b) partially broken Ni pellet surface.

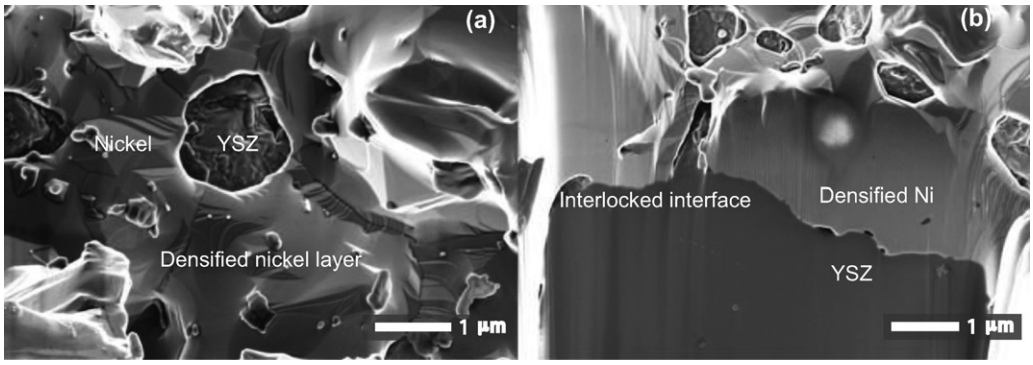

Fig. 5. (a) Top view of the densified Ni layer on YSZ substrate and (b) cross-section of the interlocked interface between Ni and YSZ.

It is shown that in the non-contacting region, Ni particle structure remained porous, while at the contacting point, certain amount of Ni was bonded to YSZ surface as clusters. Some broken YSZ pieces had been found attached to densified Ni at contacting region. The mechanical bonding between Ni and YSZ was even stronger than Ni–Ni bonding. In order to explain this bonding mechanism, cross-section of Ni–YSZ interface at contacting point was observed by SEM with larger magnification. Fig. 5(a) shows the top view of the bonding contacting area, which indicates that certain Ni at contacting point had been densified and spreading over YSZ surface after 60 h discharging with 3% H_2O. Fig. 5(b) shows the cross-section morphology of Ni–YSZ interface. With knowing that Ni has very little solid solubility in YSZ [12], it is clear to see that the Ni–YSZ mechanical bonding is due to the densified Ni and its gapless interlocking effect with rough YSZ surface. The mechanical interlocking theory states that mechanical bonding occurs when a solid penetrates into the pores, holes, crevices and other irregularities of the substrate surface, and locks mechanically to the substrate.

The microstructures of the Ni–YSZ contacting points tested in different humidity conditions are compared in Fig. 6. EDX mapping was used to identify the element distributions. For all the four cases, densified Ni layers can be found at Ni–YSZ interface. In dry hydrogen and 3% H_2O, the densified Ni layer size is much larger than those in 10% H_2O. From the clearly shown crystal boundaries, we can see that most of the Ni droplets had already merged each other in their growing process. For the cell tested in 30% H_2O, no densified Ni layer was observed along the cluster edge and only certain Ni rim was observed at Ni–YSZ contacting point within cluster. No significant impurities were found from EDX mappings for all the cases. From the comparison, it is clearly shown that with the increase of humidity in the fuel flow, densified Ni layer redistribution along the cluster edge was prohibited while the redistribution of densification Ni at Ni–YSZ contacting point within Ni cluster existed for all the cases. All the densified Ni phase shows smooth surface compared to bulk Ni.

The cross-section of the bulk porous Ni phase far from contacting layer were compared with the sample right after reduction for the three cases with humidities of 3%, 10% and 30%, as shown in Fig. 7, to study the effect of humidity on bulk Ni sintering. It is shown that, within 60 h, Ni particle coarsening happened to all the three cases compared to the state after initial reduction. Total porosity as well as sub-micron inner porosity were measured. The latter is defined as the area percentage of the pore with a diameter smaller than 1 μm which is surrounded by Ni phase. The statistic results of two porosities are shown in Fig. 8. Compared to the sample after initial reduction, total porosity increased with the increase of humidity, while the porosity of inner pore smaller than 1 μm decreased after initial reduction but kept almost constant in the three humidity conditions after 60 h.

In order to clarify the forming process of densified Ni layer, the microstructures along the edge of the bonded Ni cluster at different time steps, with a humidity of 3%, were also compared in Fig. 9. It is shown that after 10 h discharging, Ni pellet could be easily peeled off from YSZ surface without Ni clusters bonded, which means that mechanical interlocking effect between Ni and YSZ was still weak and there was no enough mechanical bonding built up after 10 h discharging. After 20 h discharging, Ni clusters started to bond to YSZ surface with strong mechanical bonding while no obvious Ni droplets can be observed. After 40 h discharging, a lot of independent Ni droplets can be observed along the edge of bonded Ni clusters. After 60 h discharging, the island Ni droplets grew and merged each other to form larger size densified Ni layer.

The corresponding A–C and C–R impedance spectra was also measured at different time steps. As shown in Fig. 10(a), it is clearly seen that for A–C impedance, both the ohmic resistance and activation polarization decrease with time. From initial to 60 h, the time ohmic resistance reduced from about 80–25 Ω, and activation polarization reduced from about 700 to 170 Ω. For C–R impedance, the ohmic resistance kept constant and the activation polarization decreased obviously with time, based on the current passage effect on LSM cathode [11].

4. Discussions

4.1. Morphological changes of Ni

Sintering is a phenomena which occurs by the diffusion of atoms through microstructure. Diffusion is caused by a gradient of chemical potential, while atoms move from a higher chemical potential to a lower one. The different paths that the atom movements follow are corresponding to different sintering mechanisms. Several typical diffusion mechanisms are: surface diffusion, vaporization transport, grain boundary diffusion, lattice diffusion and plastic deformation. Among all the mechanisms, only surface diffusion and vaporization transport can be influenced by surface adsorbed specie, like humidity in our experiments. Besides, these two mechanisms are non-densifying, while they take atoms from the surface and rearrange them onto another surface or part of the same surface. These mechanisms simply rearrange inner pores and do not cause inner pore densification. The rest of the mechanisms in sintering process are mainly dominated by temperature, mechanical pressure, sintering time and so on [13]. As the above parameters were all kept constants in our experiments, this paper focuses only on the study of surface diffusion mechanism enhanced by humidity and the vaporization transport mechanism driven by humidity gradient.

Based on the experimental observations, two typical morphological changes of Ni can be concluded. First is the enhanced sintering of Ni near TPB which is dominated by the local high

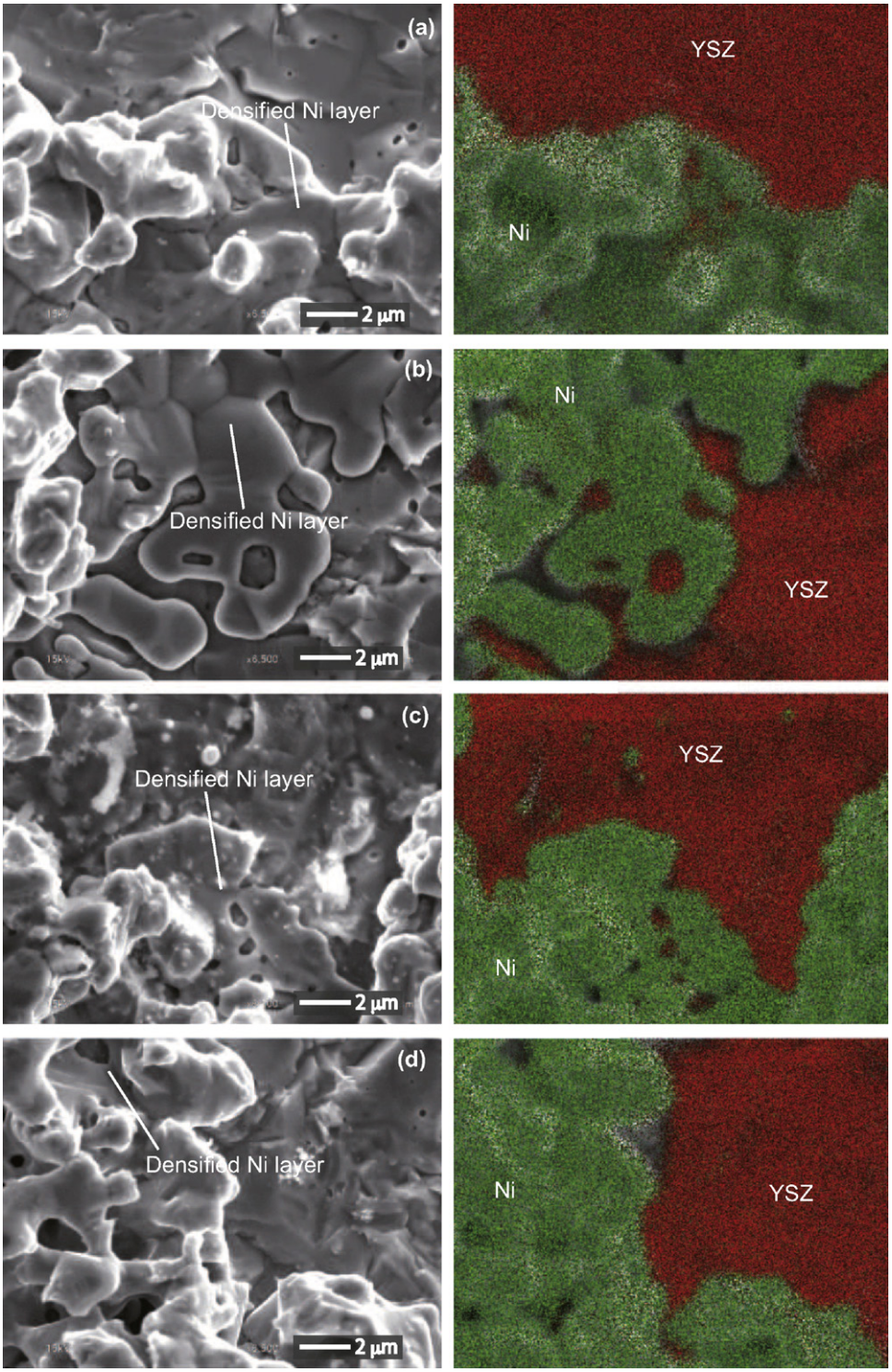

Fig. 6. Ni phase morphology and corresponding EDX mappings along Ni clusters bonded to YSZ surface after 60 h discharging, anode–cathode terminal voltage 0.6 V, in hydrogen with: (a) no H_2O, (b) 3% H_2O, (c) 10% H_2O and (d) 30% H_2O.

humidity concentration in discharging process, as shown in Fig. 5 at Ni–YSZ contacting point and in Fig. 7 for bulk Ni. Second is the phenomena of Ni droplets which is formed by vaporization–deposition mechanism driven by humidity gradient near TPB, as shown in Fig. 4.

4.1.1. Interlocking and spreading of densified Ni layer

Economos and Kingery [12] studied the interactions between different metals and oxides. In their study, Ni and zirconia were heated up to 1800 °C in reduced gas environment until Ni melted. No apparent reaction took place at Ni–zirconia interface, while Ni adhered to zirconia substrate by mechanical interlocking effect. No chemical reaction was observed at metal–ceramic interface and melted Ni cannot wet zirconia surface. In our experiments, the operating temperature setting was too low to achieve metal–ceramic interlocking effect by thermally melting Ni phase onto YSZ substrate. Mechanical interlocking phenomena was indeed observed after 60 h discharging.

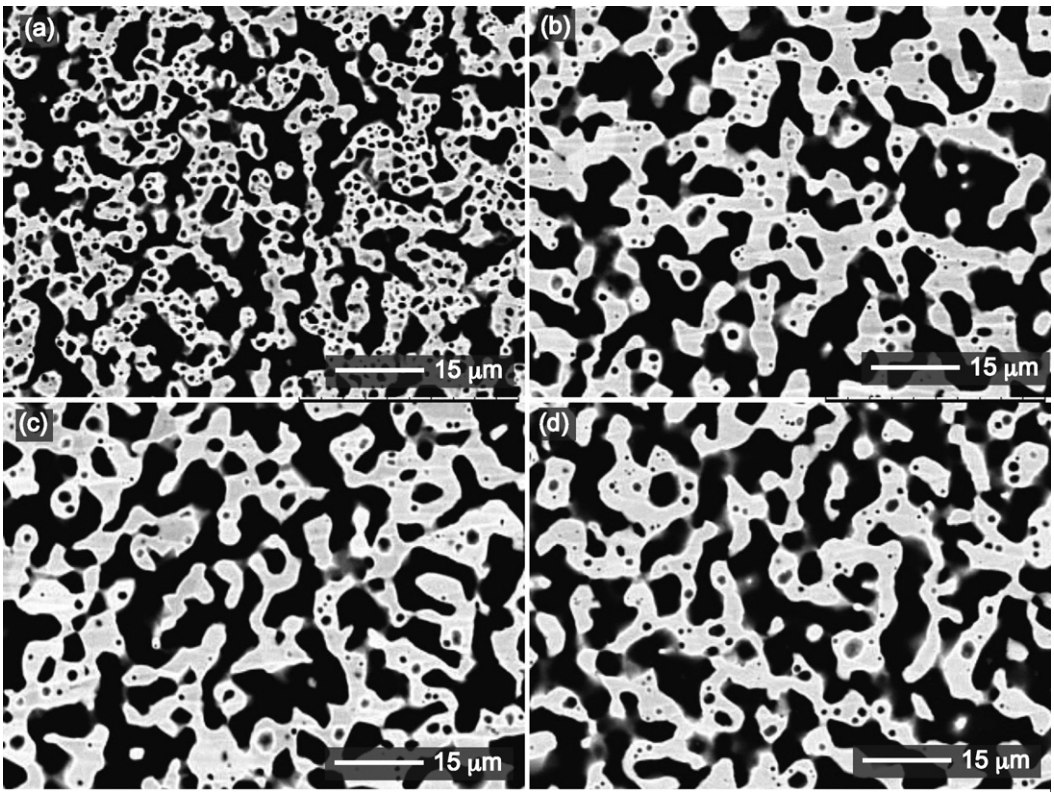

Fig. 7. Cross-sectinal images of bulk Ni phase: (a) after initial reduction, (b) after 60 h discharging in hydrogen with 3% H_2O, (c) 10% H_2O and (d) 30% H_2O.

Some researchers have tried to develop a computational model which can represent the coupled behavior of the elementary chemistry, electrochemistry and transport in the vicinity of SOFC TPB on Ni surface. The interactions of hydrogen, steam and Ni surface were widely studied [4,11]. Ni surface adsorbed species include hydrogen atom, oxygen atom and hydroxyl species and the charge transfer process is accomplished by the spillover effects of these species between Ni and YSZ surfaces [4], which is shown in Fig. 11. The potential oxygen adsorption-desorption reaction is always neglected because oxygen bonds strongly to Ni surface and cannot desorb as oxygen molecular especially when hydrogen atom is available that Ni surface adsorbed water molecular can be formed. Under ordinary SOFC anode operating conditions, the gas-phase oxygen partial pressure is so low that oxygen adsorption is usually unimportant. Jens et al. [14] have shown that Ni–OH bonding has a much lower energy of formation than Ni adatoms on Ni surface in different temperatures. In their studies, it was considered that in humidified reduction environment at high temperature, hydroxyl species can exist stably on Ni surface. They concluded that in steam/hydrogen mixtures, hydroxyl bonded Ni dimers (a dimer is defined as a chemical entity consisting of two structurally similar subunits, which are joined by bonds, which can be strong or weak) dominated the surface diffusion of Ni particles and consequent sintering via particle migration and coalescence. The sintering rate in humidified reduction environment then can be accelerated to hundreds of times more than conventional thermal sintering. This explains the fast densification of Ni and interlocking effect within a relatively low operation temperature in discharging process. It has been shown in Section 1 that the H_2O concentration near TPB can be very different from bulk gas in discharging. With a lower A–C terminal voltage, high electrochemical reaction efficiency may create high humidity concentration atmosphere at TPB, which results in the accelerated surface diffusion enhanced sintering of Ni at Ni–YSZ interface. The sintering process finally leaded to the fast interlocking between Ni and YSZ in a short time and low temperature discharging. As shown in Fig. 11, in the the surface diffusion process, surface Ni atom bonded by hydroxyl species always traveled towards surface with large curvature which has lower chemical potential. In the sintering process, the enhanced surface diffusion finally filled all the pores, holes, crevices and other irregularities of Ni at Ni–YSZ interface and the YSZ substrate. The filling of Ni into all the substrate YSZ irregularities finally resulted in interlocking.

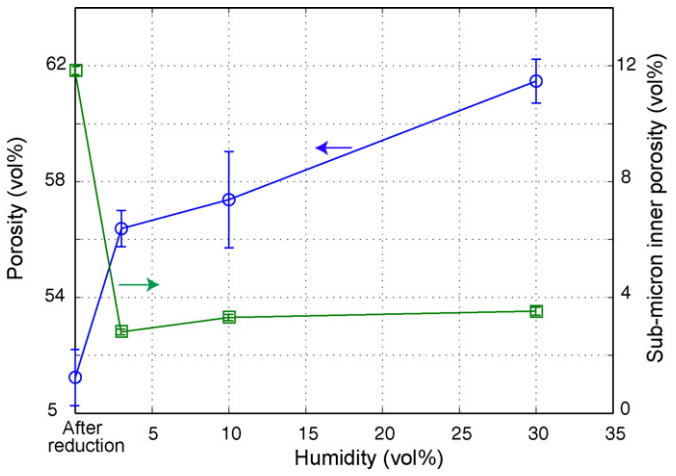

Fig. 8. Bulk Ni phase porosity and sub-micron inner porosity versus hydrogen humidity.

For bulk Ni, the total porosity after 60 h discharging increased and the sub-micron inner porosity was kept almost constant with the increase of humidity, as shown in Fig. 8. Because the samples of bulk Ni were taken far from Ni–YSZ contacting layer, the influence of humidity generated in the chemical reactions can be ignored.

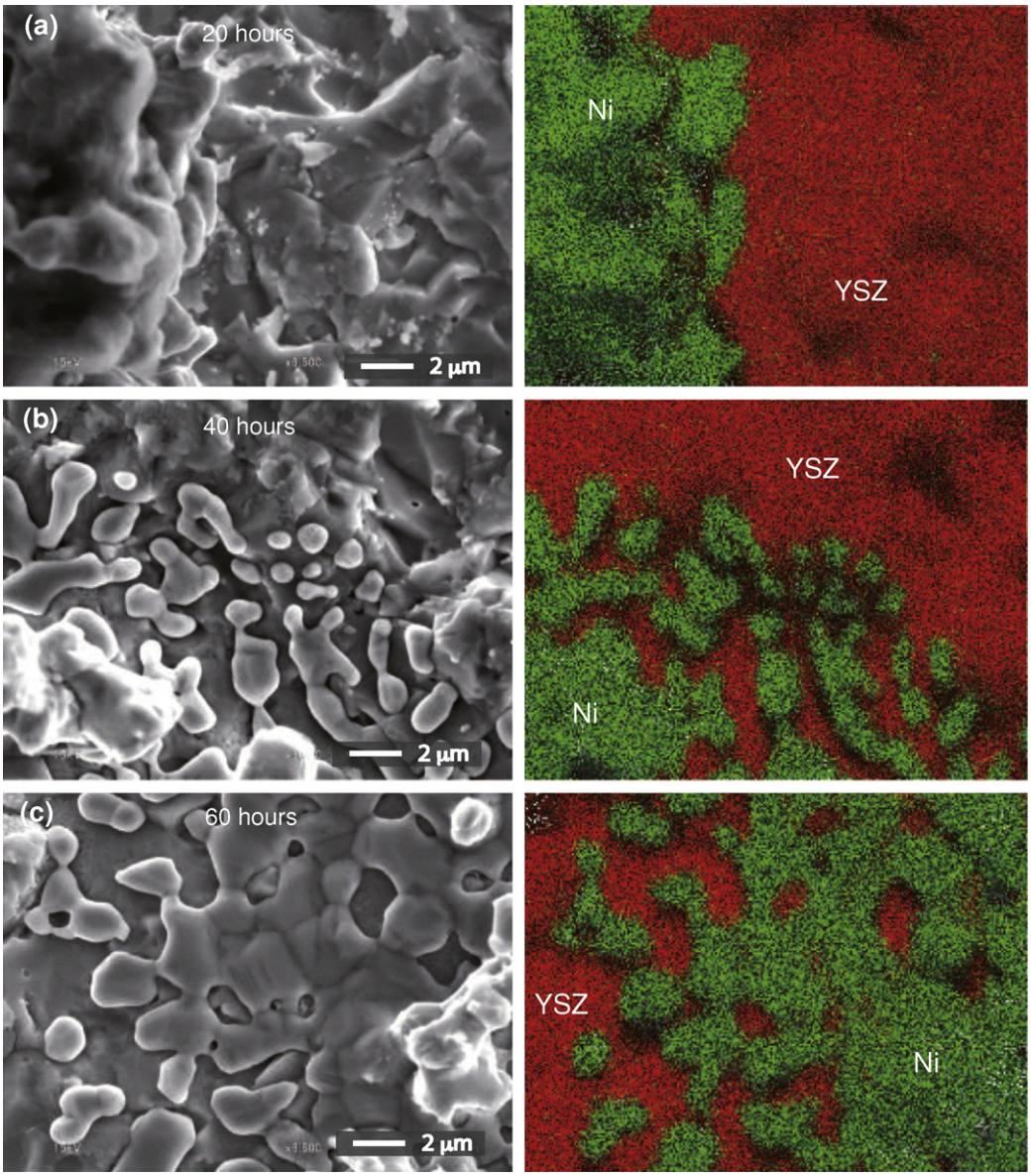

Fig. 9. Ni phase morphology and corresponding EDX mappings along TPB after: (a) 20 h, (b) 40 h and (c) 60 h (3% H_2O, 97% H_2).

The sintering of Ni in all the three samples tested in humidified hydrogen environments were dominated by the bulk gas humidity enhanced surface diffusion only. Because the inner pore has no contact with the bulk gas, the sintering was mainly dominated by temperature caused densifying factors so that similar values were obtained after discharging. The results supports the enhancement of Ni sintering dominated by hydroxyl species on Ni surface within humidified hydrgen.

4.1.2. Vaporization–deposition phenomena of Ni caused by humidity gradient

It is known from thermodynamic data that the standard Gibbs free energy ΔG° of Ni surface adsorbed hydroxyl species is lower than those of surface adsorbed hydrogen and oxygen in high temperture [4]. The hydroxyl species has been proven to exist as $Ni(OH)_2$ layer [15]. Matsui et al. [2] calculated the molar fraction of volatile Ni species in humidified hydrogen atmosphere at 1000 °C. The calculation showed us that 20% mole fraction of humidity in hydrogen is a critical value above which the mole fraction of volatile $Ni(OH)_2$ is more than both NiO and Ni. The Ni–YSZ interface microstructures after different discharging times shown in Fig. 9 give the evidence for the assumption of Ni vaporization–deposition mechanism. Simner et al. [16] have shown that metal vaporization–deposition and accumulation at reducing TPB happen with in SOFC cathode when Pt or Ag current collectors were used. In our paper, most of the Ni droplets were found to be independent islands after 40 h discharging within 3% H_2O, which means that Ni droplets cannot be formed by surface diffusion which must result in continuous Ni layer.

de Boer et al. [17] have tested SOFC with porous Ni electrode prepared by electron-beam evaporation technique. The smooth Ni droplets found in our experiment has similar morphology as the electrode deposited by electron-beam evaporation method, with very smooth surface. This also supports the assumption that the Ni droplets in our experiment were formed by vaporization–deposition mechanism. Similar redistribution phenomena has also been reported by Brown et al. [8,9]. In their researches, Ni wire point-electrode was applied by mechanical pressing against ScSZ electrolyte. The accumulation phenomena was explained by the dynamic accumulation of impurities and

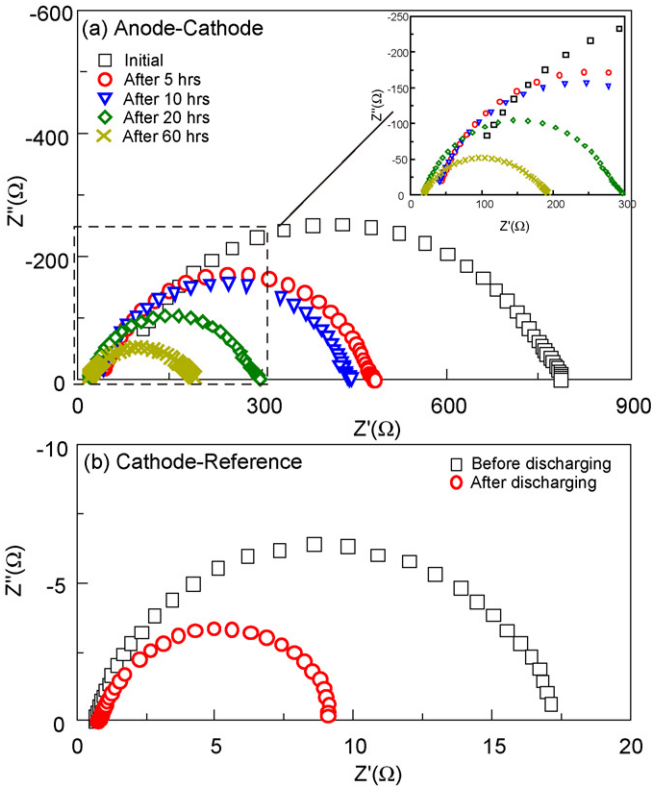

Fig. 10. (a) Anode–cathode impedance spectra after different discharging times (3% H_2O, 97% H_2) and (b) cathode–reference impedance spectra before and after 60 h discharging.

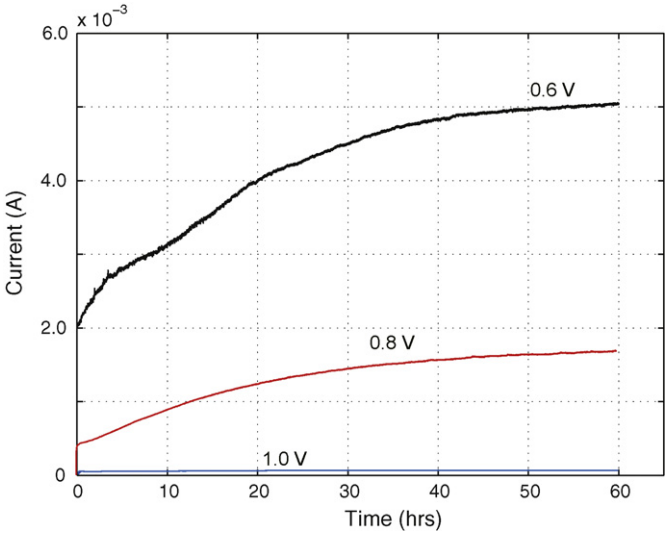

Fig. 12. Cell performance tested with different anode–cathode terminal voltages within 60 h (3% H_2O, 97% H_2).

deposited Ni at the vicinity of TPB. However, no systematical work was carried out to supply the solid evidence. In our experiments, no significant impurities were found in EDX mappings. In the initial state (before 20 h), small nucleus should be formed on YSZ surface near TPB, while the size of the small nucleus is out of the resolution limitation of EDX device so that no deposited Ni droplets are shown in Fig. 9(a). Further study should be conducted to study the formation of Ni nucleus at the beginning of the discharging process.

$$Ni(OH)_2(g) \rightleftharpoons NiO(s) + H_2O(g) \quad (1)$$

$$NiO(s) + H_2 \rightleftharpoons Ni(s) + 2H_2O(g) \quad (2)$$

The deposition process can be described by Eqs. (1) and (2). Belton and Jordan [18] have studied the gaseous hydroxides of Ni and measured the volatilization reaction standard Gibbs energy changes of the reactions shown in Eqs. (1) and (2). It was proved that gaseous hydroxides of Ni increase with the partial pressure of humidity in hydrogen. It has been shown in Section 1 that the H_2O concentration near TPB can be very different from bulk gas flow, so that local H_2O concentration gradient can be formed outwards from near TPB to bulk gas environment. On Ni surface near TPB,

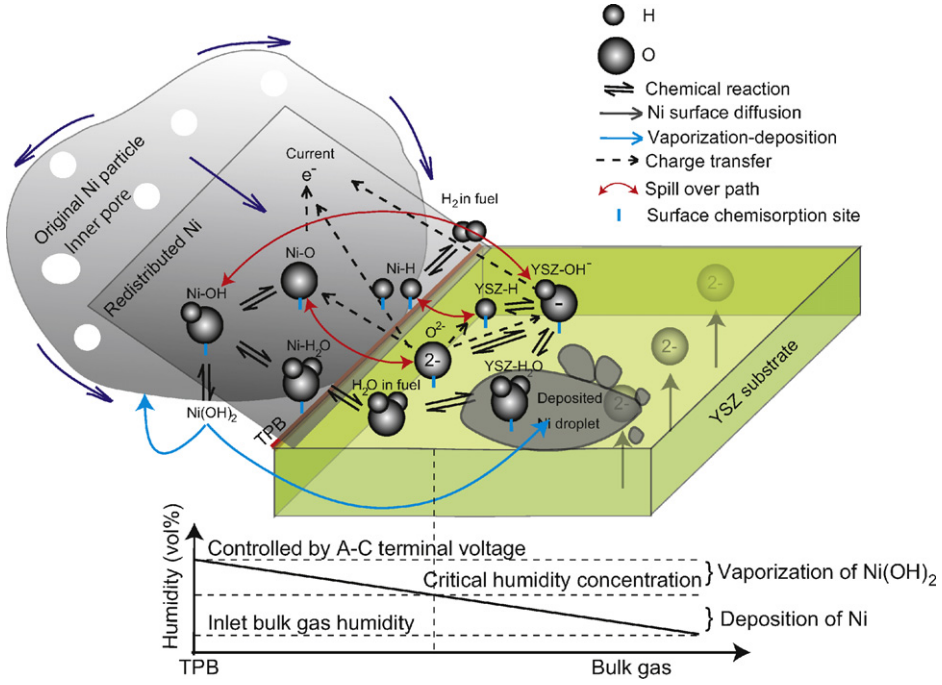

Fig. 11. Illustration of local Ni densification and vaporization–deposition processes at TPB.

high concentration of H_2O during discharging may drive the reaction to the left hand side of Eq. (1). Relatively high concentration of $Ni(OH)_2$ can be formed on Ni surface and then vaporize from Ni surface. The humidity concentration gradient then drives the volatile $Ni(OH)_2$ outwards from TPB. Once $Ni(OH)_2$ leaved Ni surface and traveled with humidity gradient to a lower humidity environment, gas state $Ni(OH)_2$ was then deposited onto YSZ surface reduced to Ni. With this redistribution phenomena of Ni continuing, the deposited Ni droplets kept growing and merged to each other and finally formed a dense Ni layer which was firmly interlocked to YSZ surface.

Fig. 11 shows the illustration of the vaporization–deposition process. The critical value of mole fraction of humidity in hydrogen above which volatile $Ni(OH)_2$ can exist stably over Ni and NiO is estimated to be larger than 20%, when the temperature was lower than 1000 °C [2]. In these discharging experiments, spreading of densified Ni layer caused by merging of Ni droplets phenomena can only be observed when the bulk gas was dry or humidified by 3% H_2O and 10% H_2O. No such phenomena was observed when the gas was humidified by 30% H_2O. So that the critical value of mole fraction of humidity in hydrogen in our measurements can be estimated to be a value between 20% and 30%. 30% H_2O cannot cause the deposition of Ni near TPB even there was certain humidity gradient, because Ni hydroxide can exist stably in the gas environment and only enhanced the bulk Ni surface diffusion with a high surface concentration of Ni surface adsorbed hydroxyl specie. For the cells tested in hydrogen, which was dry, humidified by 3% H_2O and 10% H_2O, the deposition phenomena was prohibited by the increase of humidity because of the decreasing humidity gradient from TPB to bulk gas when the terminal voltage was fixed, which is shown in Fig. 6. For dry hydrogen, densified Ni layer almost without gap was observed after discharging testing. Clear crystal boundary indicated the merging and growing of small Ni droplets. For hydrogen humidified by 3% H_2O, similar phenomena can be observed while more gaps and much more clear grain boundary existed at the same time. For hydrogen humidified by 10% H_2O, only a little densified Ni layer can be observed very close to contacting point. For hydrogen humidified by 30% H_2O, no spreading of densified Ni layer was observed along the edge of cluster. What is common for all the four testings is that densified Ni redistribution can be found at Ni–YSZ interface within Ni clusters which resulted in the interlocking effect. In last section, we have introduced the enhancement of

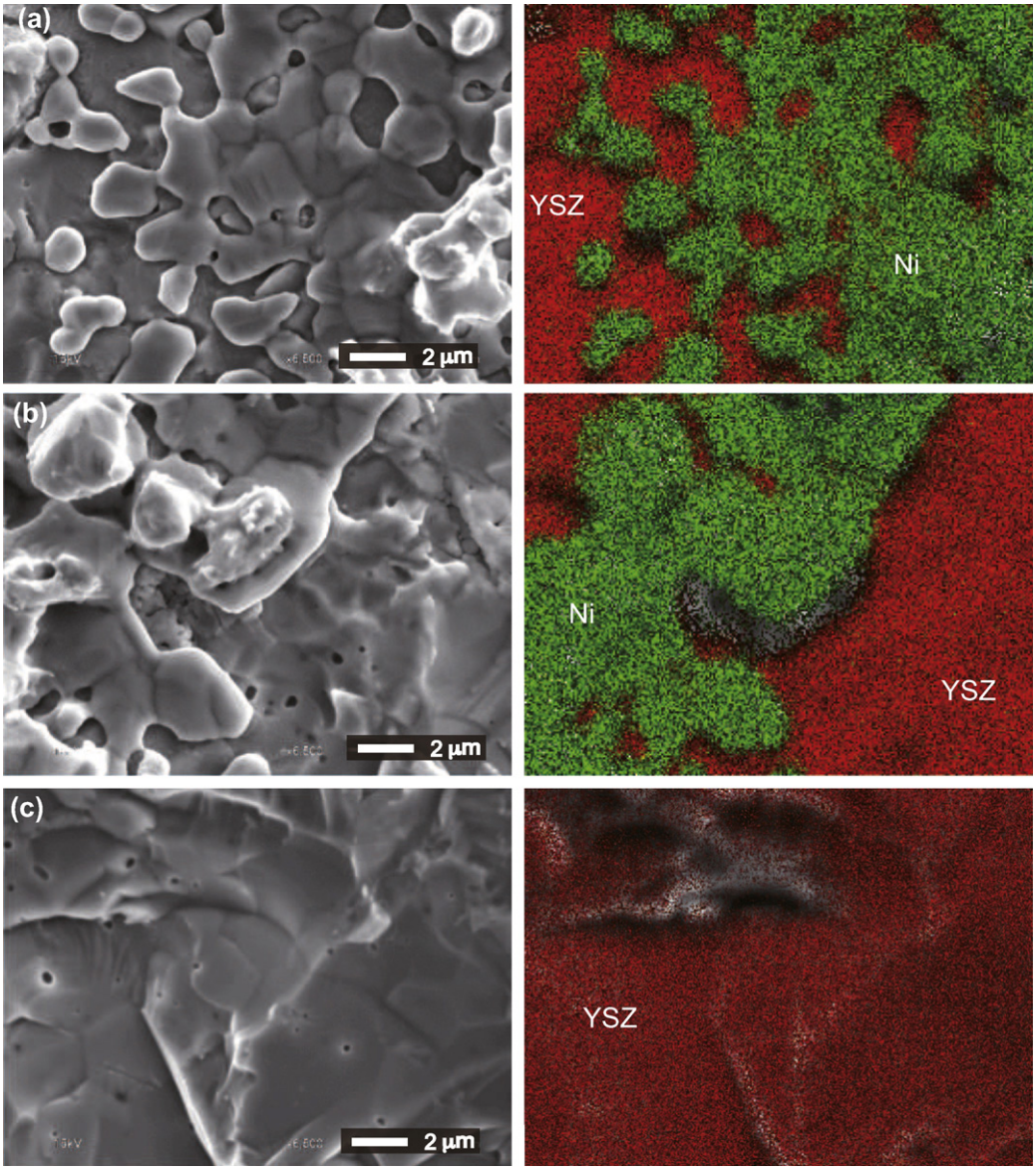

Fig. 13. Ni morphology and corresponding EDX mappings along TPB after 60 h discharging with different anode–cathode terminal voltages: (a) 0.6 V, (b) 0.8 V and (c) 1 V (3% H_2O, 97% H_2).

Ni surface diffusion by high concentration humidity near TPB which accelerated the local sintering of Ni and caused mechanical interlocking. The vaporization–deposition mechanism introduced in this section may also contribute to the fast sintering of Ni near TPB in the discharging process within bonded cluster. Inside the cluster, because of symmetric microstructure that every Ni–YSZ contacting point is surrounded by others, no humidity gradient presents like the edge of the bonded cluster. The local vaporization–deposition can only happen along the direction perpendicular to YSZ substrate towards bulk Ni, which can also enhance the local morphological changes of Ni.

4.2. Further study on Ni vaporization–deposition phenomena with different A–C terminal voltages

In order to further investigate the influence of local humidity on Ni morphological changes and humidity gradient at TPB on Ni vaporization–deposition mechanism, terminal voltages were varied and bulk gas humidity was fixed at 3%. Fig. 12 shows the performances of the cells tested with different A–C terminal voltages of 0.6, 0.8 and 1.0 V. It is clearly shown that higher terminal voltage resulted in more stable performance. The microstructures of the three cells after 60 h discharging were compared. Interlocking and densified Ni layer redistribution phenomena were observed for both 0.6 and 0.8 V. For 1.0 V, no Ni cluster was bonded onto YSZ surface, which means that interlocking effect was very weak with high terminal voltage in the discharging process. The performance at 1.0 V also shows that the mechanical force of the spring in our measurement was stable that all the variations of performance were not due to the unstable mechanical pressing force. The corresponding microstructures of cells at the edge of attached Ni cluster after discharging are presented in Fig. 13. It is shown that, lower terminal voltage causes larger scale densified Ni layer spreading along TPB, which proves the assumption that Ni redistribution based on vaporization–deposition cycle is driven by humidity gradient outwards from TPB to bulk gas. With higher terminal voltage setting, the local humidity at TPB was too low to enhance the Ni surface diffusion and produce volatile Ni hydroxide, so that no spreading of densified Ni layer can be observed and even no interlocking bonding was formed between Ni and YSZ surface because of low local humidity concentration.

4.3. Correlation of the Ni morphological changes to the cell performances

The mechanisms of the redistribution of Ni and the morphological change of bulk Ni structure described above can be used to explain the cell performances within different humidified fuel environments shown in Fig. 3. The increases of performances in dry hydrogen, 3% H_2O and 10% H_2O are due to fast interlocking effect and the Ni spreading along TPB, which enlarges the effective TPB length and reduces interface ohmic resistance. The corresponding A–C impedance spectra measured at different time steps in 3% H_2O, as shown in Fig. 10(a), supports this explanation. According to Fig. 6, the spreading rate of densified Ni layer caused by Ni droplets merging is much faster when the bulk gas humidity is dry and 3% than 10%. This explains the different increasing rates of dry hydrogen, 3% H_2O and 10% H_2O. For the cell performance tested within 30% H_2O, the short step of extremely fast increase of the initial cell performance is due to the fast interlocking effect at Ni–YSZ interface enhanced by the high bulk gas humidity (30% H_2O). The decrease of Ni surface activation overpotential at TPB within high bulk gas humidity [2,19] also contributed to the fast increase. The following irregular performance is due to the competition between the fast sintering of bulk Ni enhanced by high humidity and the continuous interlocking effect between Ni and YSZ. For the oscillation signal observed, similar phenomena has been reported by Hauch et al. [20]. Local tension can be built up by fast interlocking effect at TPB in high humidity environment. The coarsening of bulk Ni as shown in Fig. 8 also influenced the cell performance by changing mechanical force at contacting point.

It is considered that in conventional Ni–YSZ composite cermet anodes, low bulk gas humidity may accelerate the degradation of anode at TPB by enhancing the redistribution of Ni by deposition while high bulk gas humidity may accelerate the degradation of bulk Ni by enhancing the coarsening rate of the whole Ni network [2]. In the future study, quantified analysis will be carried out to investigate the relationships between morphological changes and the local humidity at TPB.

5. Conclusions

Porous Ni pellet was used as anode in SOFC by being mechanical pressed against YSZ substrate with pure LSM cathode. The cell was discharged in different humidities environments and A–C terminal voltages. The local Ni morphological changes at Ni–YSZ contacting points and bulk Ni were studied by SEM after discharging. It was found that interlocking effect between Ni and YSZ and redistribution of densified Ni layer along TPB were formed with low discharging terminal voltages which resulted in larger local humidity concentration. Along the edge of Ni clusters interlocked to YSZ surface, the phenomena of the growing and merging of Ni droplets was observed. As humidity at TPB can be very different from that in bulk gas with in discharging process, it is considered that the local morphological changes of Ni at TPB were mainly caused by both humidity enhanced surface diffusion of Ni and the vaporization–deposition mechanism of $Ni(OH)_2$ driven by humidity gradient outwards from TPB to bulk gas environment. The competition of local and bulk Ni morphological changes finally influenced the anode transient discharging performances. Further research should be conducted to quantify the Ni–YSZ interactions in discharging process by using 3D reconstruction technique [21], and relevant electrochemical analysis should be carried out to study the morphological changes quantitatively.

Acknowledgment

This work was supported by the New Energy and Industrial Technology Development Organization (NEDO) under the Development of System and Elemental Technology on Solid Oxide Fuel Cell (SOFC) Project.

References

[1] S. Koch, P.V. Hendriksen, M. Mogensen, Y.-L. Liu, N. Dekker, B. Rietveld, B.D. Haart, F. Tietz, Fuel Cells 2 (2006) 130–136.
[2] T. Matsui, R. Kishida, J. young Kim, H. Muroyama, K. Eguchi, J. Electrochem. Soc. 157 (2010) B776–B781.
[3] D. Simwonis, F. Tietz, D. Stover, Solid State Ionics 132 (2000) 241–251.
[4] D.G. Goodwin, H. Zhu, A.M. Colclasure, R.J. Kee, J. Electrochem. Soc. 156 (2009) B1004–B1021.
[5] V. Marcel, B.-H. Anja, G. Ludwig, W. Jurgen, G.B. Wolfgang, J. Electrochem. Soc. 156 (2009) B663–B672.
[6] K.V. Hansen, K. Norrman, M. Mogensen, J. Electrochem. Soc. 151 (2004) A1436–A1444.
[7] J. Mazusaki, H. Tagawa, T. Saito, T. Yamamura, Solid State Ionics 70–71 (1994) 52–58.
[8] M. Brown, S. Primdahl, M. Mogensen, J. Electrochem. Soc. 147 (2000) 475–485.
[9] M.S. Schmidt, K.V. Hansen, K. Norrman, M. Mogensen, Solid State Ionics 180 (2009) 431–438.
[10] R.J. Aaberg, R. Tunold, M. Mogensen, R.W. Berg, R. Odegard, J. Electrochem. Soc. 145 (1998) 2244–2252.
[11] S.P.S. Badwal, M.J. Bannister, R.H.J. Hannink, Science Technology of Zirconia V, Technomic Publishing Company, 1993.
[12] G. Economos, W.D. Kingery, J. Am. Ceram. Soc. 36 (1952) 403–409.
[13] J. Sehested, J. Catal. 217 (2003) 417–426.

[14] J. Sehested, J.A. Gelten, I.N. Remediakis, H. Bengaard, J.K. Norskov, J. Catal. 223 (2004) 432–443.
[15] N. Kitakatsu, V. Maurice, C. Hinnen, P. Marcus, Surf. Sci. 407 (1998) 36–58.
[16] S.P. Simner, M.D. Anderson, L.R. Pederson, J.W. Stevenson, J. Electrochem. Soc. 152 (2005) A1851–A1859.
[17] B. de Boer, M. Gonzalez, H.J.M. Bouwmeester, H. Verweij, Solid State Ionics 127 (1999) 269–276.
[18] G.R. Belton, A.S. Jordan, J. Phys. Chem. 71 (1967) 4114–4120.
[19] S.P. Jiang, Y. Ramprakash, Solid State Ionics 116 (1999) 145–156.
[20] A. Hauch, S.D. Ebbesen, S.H. Jensen, M. Mogensen, J. Electrochem. Soc. 155 (2008) B1184–B1193.
[21] H. Iwai, N. Shikazono, T. Matsui, H. Teshima, M. Kishimoto, R. Kishida, D. Hayashi, K. Matsuzaki, D. Kanno, M. Saito, H. Muroyama, K. Eguchi, N. Kasagi, H. Yoshida, J. Power Sources 195 (2010) 955–961.